Supplementary Figures

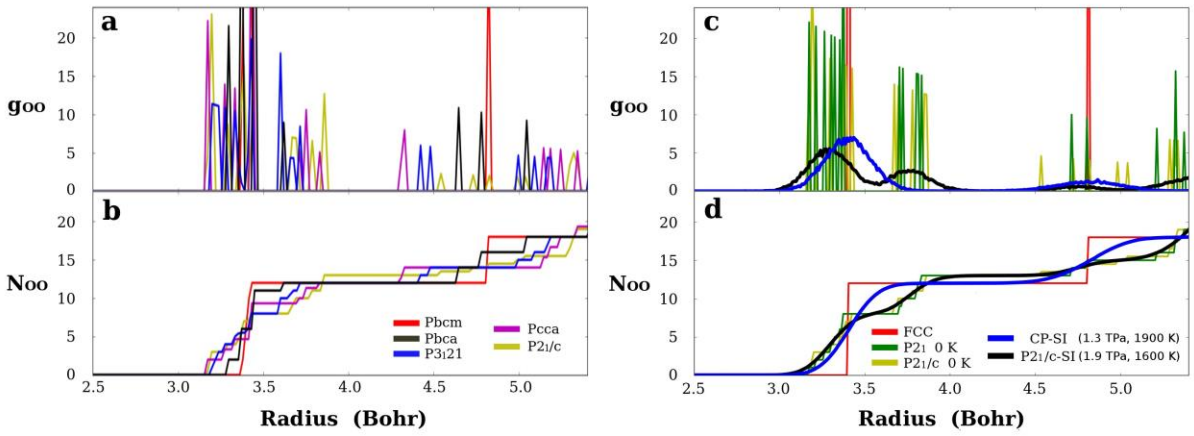

Supplementary Figure 1: Pair correlation function and coordination number of the oxygen sublattice. (**a**) Pair correlation function for the static structures Pbcm, Pbca, $P3_121$, Pcca, and $P2_1/c$. (**b**) Coordination number for the static structures Pbcm, Pbca, $P3_121$, Pcca, and $P2_1/c$. (**c**) Pair correlation function for CP-SI and $P2_1/c$-SI. (**d**) Coordination number for CP-SI and $P2_1/c$-SI. The corresponding quantities for the static $P2_1$ and $P2_1/c$ structures and the ideal FCC lattice are also given for comparison. (**a**) and (**b**) illustrate the systematic changes that occur in the O sublattice with increasing pressure.

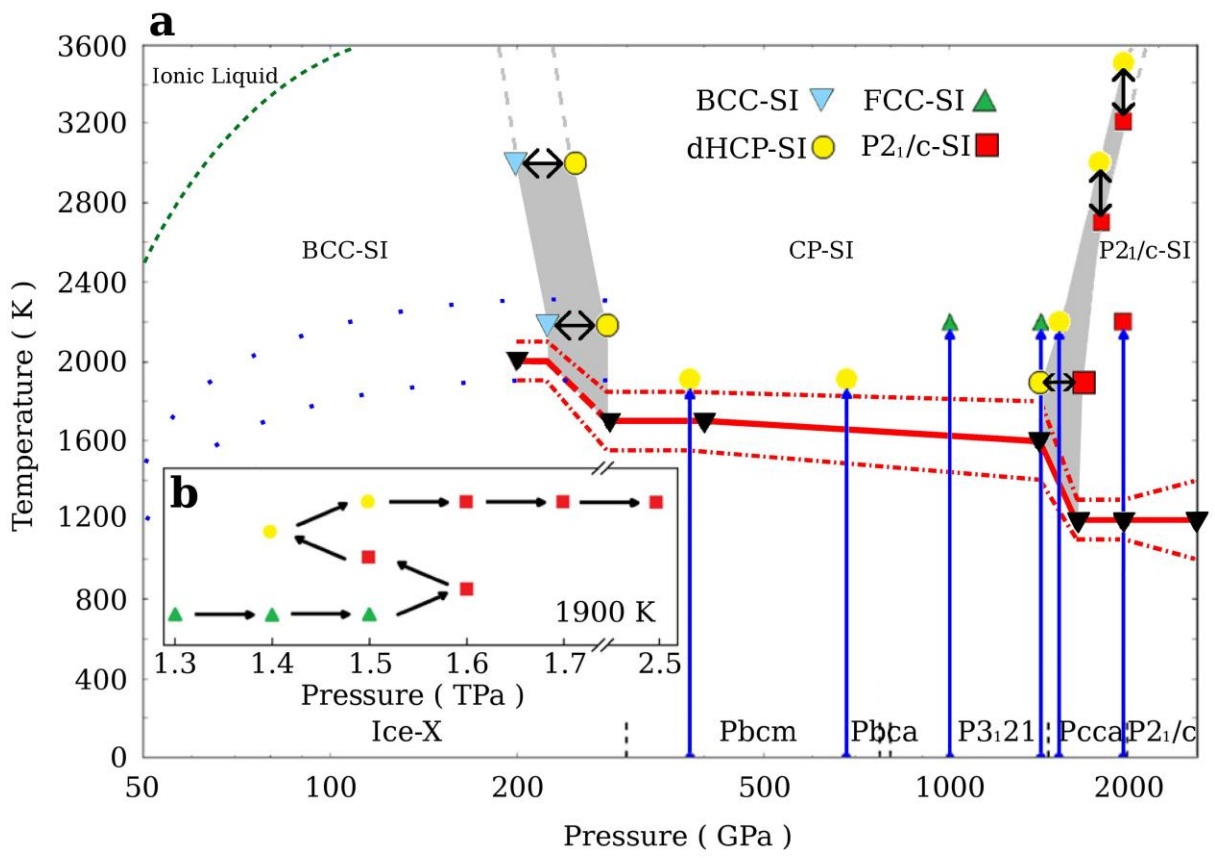

Supplementary Figure 2: The detailed superionic phase diagram. (**a**) Phase diagram. The hydrogen sublattice melting curves below 200 GPa (blue dots) are taken from [1]. We find they arein agreement with our predicted melting temperature at 200 GPa. The black triangles and solid red lines indicate the melting temperature of the H sublattice, ignoring quantum effects. The red dot- dash lines indicate the standard error of the melting temperature estimated by simulated annealing cycles. The gray area indicates the superionic phase boundary and the associated uncertainty. Thesimulation data indicate a likely negative slope of the BCC-SI to CP-SI boundary and positiveslope of the CP-SI to $P2_1/c$-SI boundary. As discussed in the main article it is very plausible thatthe slope of the melting line be negative in correspondence with the two sharp drops of the meltingtemperature. The solid blue lines show the transition starting from zero-temperature structures. It is interesting to note that depending on the pressures, the final superionic phase starting fromPcca can be both CP-SI and $P2_1/c$-SI. The black dashed vertical lines indicate phase boundariesat zero K according to [2]. (**b**) The reversible transition between CP-SI and $P2_1/c$-SI.

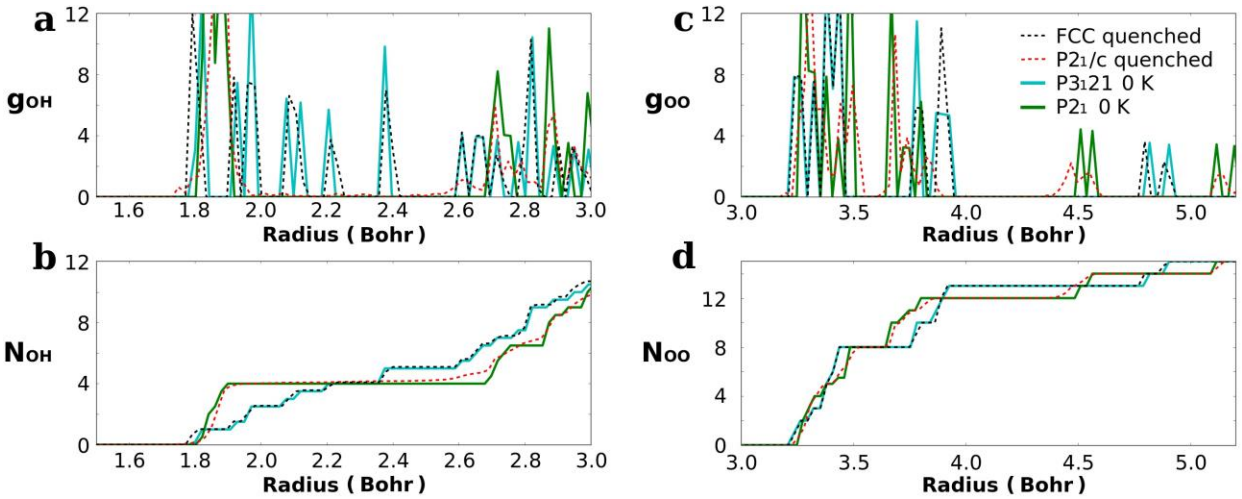

Supplementary Figure 3: Pair correlation functions and coordination numbers of quenched structures. (**a**) OH pair correlation functions. (**b**) OH coordination numbers. (**c**) OO pair correlation functions. (**d**) OO coordination numbers. Structures quenched from supe- rionic phases at (T = 1900 K, P = 1.3 TPa) and (T = 1900 K, P = 1.9 TPa) are compared with $P3_121$ and $P2_1$ zero K structures. The minor differences between the quenched and the equilibrium 0 K structures reflect the accuracy of the final steepest descent minimization that we apply to the quenched structures at 200 K.

Supplementary Table 1

Supplementary Table 1: Effective charge tensor in two SI phases.

Structure	Atom	$< Z_0 >$	$L=0$	$L=1$	$L=2$
$P2_1/c$-SI	O	-2.4 ± 0.2	85%	4%	11%
	H	1.2 ± 0.1	71%	3%	26%
CP-SI	O	-2.4 ± 0.2	80%	5%	15%
	H	1.2 ± 0.1	60%	3%	37%

Supplementary Notes

Supplementary Note 1

We decompose the charge tensor into three parts, according to the representations of the spatial rotations [3]. Among them, L=0 is the isotropic part, which is given by the trace of the charge tensor. L=1 and L=2 are the anisotropic parts, which correspond to the antisymmetric and to the traceless symmetric decomposition of the charge tensor, respectively. The magnitude of each component can be quantified with the 2-norm for matrices. Supplementary Table 1 summarizes the results. L=0 is the dominant component in both phases. There is also a large contribution from the L=2 part, especially for H.

Supplementary Note 2

We adopt the norm-conserving pseudopotentials which were generated according to the proce- dures detailed by Hamann-Schlueter-Chang [4] and Vanderbilt [5]. The pseudopotentials can be downloaded at http://fpmd.ucdavis.edu/potentials/index.htm. For O, the p channel is the local reference and the pseudopotential includes a nonlocal s channel. The H pseudopotential is local and regular at the origin. The transferability of these pseudopotentials can be gauged by com-paring the ground-state radial atomic pseudowavefunction $u(r) = rR(r)$ ($\int_0^\infty u(r)^2 dr = 1$) and its corresponding all electron (AE) counterpart. For O, we find that the 2s and 2p radial atomic pseudowavefunctions coincide with their AE counterparts when r is greater or equal to 1.1 Bohr, while for H the 1s radial pseudowavefunction is essentially indistinguishable from its non-pseudized counterpart all the way to the origin (where the pseudized $R(r)$ lacks the cusp of the non-pseudized $R(r)$). The regions in which the pseudowavefunctions differ from their AE counterparts define the atomic cores. In our simulated structures, the minimum distance between two oxygens never goes below 2.8 Bohr, that between O and H never goes below 1.5 Bohr and that between two H never goes below 1.4 Bohr. We infer that the adopted pseudopotentials should be adequate since core overlap never occurs at the thermodynamic conditions of our simulations. As a further test we check that with our adopted pseudopotentials the predicted phase boundaries between high pres-sure ices at zero T coincide with those reported in Supplementary Ref. [2], which used ultrasoft pseudopotentials, when ZPE is excluded.

Supplementary References

[1] Cavazzoni, C. *et al*. Superionic and metallic states of water and ammonia at giant planet conditions. *Science* **283**, 44-46(1999).

[2] Pickard, C. J., Martinez-Canales, M. & Needs, R. J. Decomposition and terapascal phases ofwater ice. *Phys. Rev. Lett.* **110**, 245701 (2013).

[3] Pasquarello, A. & Car, R. Dynamical charge tensors and infrared spectrum of amorphous SiO_2. *Phys. Rev. Lett.* **79**, 1766–1769 (1997).

[4] Hamann, D. R., Schlu¨ter, M. & Chiang, C. Norm-conserving pseudopotentials. *Phys. Rev. Lett.* **43**, 1494–1497 (1979).

[5] Vanderbilt, D. Optimally smooth norm-conserving pseudopotentials. *Phys. Rev. B* **32**, 8412–8415 (1985).